# *Structured connectivity in the output of the cerebellar cortex*

Kim M. Gruver[1,2], Jenny W. Y. Jiao[1], Eviatar Fields[1,2], Sen Song[3], Per Jesper Sjöström[4], and Alanna J. Watt[1*]

[1] Department of Biology, McGill University, Montréal, QC, Canada.

[2] Integrated Program in Neuroscience, McGill University, Montréal, QC, Canada.

[3] Laboratory of Brain and Intelligence and Department of Biomedical Engineering, Tsinghua University, Beijing, China.

[4] Department of Neurology and Neurosurgery, McGill University, Montréal, QC, Canada.

*Correspondence: alanna.watt@mcgill.ca

## Abstract

Circuits in the brain are built from connections between neurons, where the spatial organization and functional properties of these connections determines circuit function. In the cerebellum, Purkinje cells transmit information to neurons in the cerebellar nuclei, but how Purkinje cell – nuclear neuron connections are organized remains unclear. Here, we explored the connections between Purkinje cells and cerebellar nuclear neurons using whole-cell electrophysiology and optogenetics to produce spatial connectivity maps of cerebellar cortical output. We observed non-random connectivity between Purkinje cells and their target neurons, with inputs to cerebellar nuclear neurons clustering along cerebellar transverse zones. While many nuclear neurons received inputs from a single zone, a number of different connectivity motifs were observed. Neurons receiving inputs from all four zones were more common than predicted by a random model and showed topographic organization in the nucleus. Finally, we observed that small Purkinje cell inputs were sufficient to pause the output of nuclear neurons, suggesting that widespread Purkinje cell synchrony may not be necessary to influence cerebellar output. These findings reveal cerebellar nuclear neurons as an important locus of multimodal cerebellar integration.

## Introduction

Connections between neurons give rise to circuits that shape brain function. Identifying how these connections are organized is therefore necessary to understand how a circuit functions. The cerebellum is a highly conserved structure that receives input from many brain regions. In the cerebellar cortex, Purkinje cells are organized into lobules, with both neuroimaging studies and disease research suggesting that Purkinje cells in different regions of the cerebellar cortex process different types of information[1–4]. In mammals, the cerebellar cortex is subdivided into four

23 functional transverse zones[5,6] that have been associated with different patterns of gene
24 expression[7,8] and physiological properties[9,10]. These zones include the anterior (lobules II-V),
25 central (VI-VII), posterior (VIII and dorsal IX), and nodular zones (ventral IX and X).

26 As the sole output of the cerebellar cortex, Purkinje cell axons target cerebellar nuclear (CN)
27 neurons with strong inhibitory synapses. It is these CN neurons that form the vast majority of
28 output neurons from the cerebellum. Previous studies have suggested that individual CN neurons
29 receive input from ~40 converging Purkinje cells[11], and anatomical studies have shown that narrow
30 bands of neighboring Purkinje cells converge on similar areas in the CN[12]. Despite the critical role
31 that the Purkinje cell – CN neuron synapse plays in cerebellar information processing, an
32 understanding of how Purkinje cells spatially converge on CN neurons has been lacking.

33 In our study, we set out to explore how Purkinje cells inputs onto CN neurons are spatially
34 organized. We focused on the cerebellar fastigial nucleus, since neurons in the fastigial nucleus
35 receive most Purkinje cell input from the vermis[13,14]. We used electrophysiology and focal
36 optogenetic stimulation to build spatial connectivity maps of Purkinje cell inputs onto individual
37 CN neurons. We found that Purkinje cell inputs to the CN are organized along the same four
38 transverse zones that are defined during cerebellar development[7]. While many CN neurons receive
39 input from a single zone, others receive Purkinje cell input from multiple zones, and connectivity
40 between Purkinje cells and CN neurons is not random. We performed viral labeling of Purkinje
41 cells from different zones and observed that their axons terminate in close proximity within the
42 CN, providing anatomical support for our functional data. Finally, we performed both cell-attached
43 and whole-cell recordings from single CN neurons to determine how Purkinje cell synaptic inputs
44 affect CN output. We found that even small synaptic inputs could shape CN neuron output, and
45 that the amplitude of the synaptic response influenced the length of the pause in spontaneous CN

46 firing. Our findings support CN neurons as a locus of integration within the cerebellum that is
47 important for cerebellar information processing.

48

49 **Results**

50 *Mapping Purkinje cell input onto CN neurons*

51 To build functional connectivity maps of Purkinje-cell convergence onto cerebellar nuclear
52 (CN) neurons, we used transgenic mice that expressed modified Channelrhodopsin-2 in Purkinje
53 cells, (Fig. 1a-c)[15]. We recorded from CN neurons in voltage-clamp configuration and used
54 focused blue light to stimulate Purkinje cell axons at the base of individual lobules sequentially
55 from lobule II to X (Fig. 1d, Supplementary Fig. 1) to evoke inhibitory postsynaptic currents
56 (IPSCs) in CN neurons. Stimulation from single lobules often evoked no synaptic response (e.g.
57 Fig. 1d, bottom), but occasionally IPSCs with fast rise and decay time constants and low failure
58 rates were observed (Fig. 1d, bottom, Supplementary Fig. 1), consistent with previous descriptions
59 of Purkinje cell – CN synapses[15,16]. By sequentially stimulating individual lobules with focally
60 restricted light, we identified the location of functional connections between Purkinje cells and CN
61 neurons which enabled us to build connectivity maps of Purkinje cell convergence (Fig. 1d, e). As
62 a positive control, we shone light over the Purkinje cell axonal terminals directly surrounding the
63 patched CN neuron soma and were able to produce large IPSCs (Fig. 1d, Axonal terminals;
64 Supplementary Fig. 1), since approximately half of CN neurons received no synaptic input from
65 lobule stimulation within the acute slice plane (Supplementary Fig. 2).

66 Determining whether Purkinje cells from a single lobule or multiple lobules (Fig. 1f)
67 converge on an individual CN neuron has important implications for cerebellar function. We found
68 that ~50% of CN neurons that produced IPSCs following lobule stimulation received input from

69 Purkinje cells located in a single lobule (Fig. 1g), while the remaining ~50% of CN neurons
70 received Purkinje cell input from between two and five lobules (Fig. 1h). We found no differences
71 in IPSC amplitudes from single-lobule stimulation in CN neurons compared with those receiving
72 multi-lobule input (Fig. 1i; Supplementary Fig. 1), suggesting that the total number of spatially-
73 distinct inputs does not influence the strength of connections from a single lobule. Furthermore,
74 the cumulative IPSC amplitude for the total input across lobules increased with the number of
75 lobules from which a cell received input (Fig. 1j). To address whether there were differences in
76 the subcellular location of Purkinje cell inputs onto CN neurons, we examined the disparity index[17]
77 of both IPSC amplitudes and rise times. We found no differences in the properties of IPSCs for
78 individual CN neurons based on the number of connected lobules (Supplementary Fig. 1). These
79 findings suggest that both single-lobule and multi-lobule innervation patterns are observed in
80 Purkinje cell convergence on CN neurons.

81 Anatomically defined lobules of the cerebellar cortex are not discrete processing units[1,5].
82 Rather, the cerebellar cortex has been subdivided into four major transverse functional zones: the
83 anterior, central, posterior, and nodular zones (Fig. 2a). Since retrograde labeling experiments have
84 shown that CN neurons receive input from narrow bands of neighboring Purkinje cells[12], we
85 hypothesized that Purkinje cells in lobules belonging to the same functional zone were more likely
86 to converge on a CN neuron than Purkinje cells in lobules from across zones. To address this, we
87 performed unsupervised hierarchical clustering analysis of our connectivity data. In agreement
88 with our hypothesis, we observed that Purkinje cells in lobules within the same functional zone
89 converged more often onto the same CN neuron than those in lobules from across zones (Fig. 2b).
90 This suggests that Purkinje cell output tends to respect the boundaries of the functional zones of
91 the cerebellar cortex.

92

93 *Connectivity motifs in Purkinje cell input onto CN neurons*

94 Do Purkinje cell inputs to CN neurons preferentially arise from single zones? As we found
95 that CN neurons can receive inputs from multiple lobules and since these lobules are grouped into
96 functional zones, we wondered whether multi-lobule innervations arose due to convergence from
97 Purkinje cells within the same zone. To address this, we looked at convergence properties of CN
98 neurons and found both single-zone and multi-zone convergence (Fig. 2c). We observed no
99 differences in IPSC amplitudes or other properties between CN neurons innervated by different
100 zones or numbers of zones (Fig. 2d; Supplemental Fig. 1), suggesting that there is no zone that
101 forms a systematically stronger input onto CN neurons. We found that multi-zonal input was not
102 rare: over a third of CNs received multi-zone input (Fig. 2e, inset). Different connectivity patterns
103 appear with different frequencies in our dataset (Supplemental Fig. 3), suggesting the existence of
104 non-random connectivity motifs.

105 To determine whether Purkinje cells converge across zones on individual CN neurons in
106 non-random motifs[18,19], we used a random model that assumes Purkinje cell connectivity from
107 each zone occurs independently of other zones and determined how well it describes our data (Fig.
108 2e). We found that four-zone convergence occurred in our dataset ~18 times more often than
109 predicted by the model, and three-zone connections trended toward significant over-representation
110 as well. This over-representation suggests that a four-zone connectivity motif may be an important
111 feature of cerebellar information transfer, and by extension, that the CN may be an important locus
112 of information integration in the cerebellum.

113

114 *No morphological signature for CN neurons with different input patterns*

115 Different classes of CN neurons have been distinguished by their morphological and
116 physiological properties[20]. To determine whether differences in morphological properties can be
117 used to classify CN neurons with different connectivity patterns, we filled CN neurons with
118 AlexaFluor 594 and performed two-photon imaging of filled cells after characterizing their
119 synaptic inputs (Fig. 3a). To characterize their physiological properties, we sampled their
120 spontaneous firing in cell-attached mode prior to recording synaptic input (Fig. 3a, bottom). We
121 compared the soma area, Sholl radius, branch index, number of primary dendrites, total dendrite
122 length, and firing rate from CN neurons with different connectivity patterns and found that these
123 properties were indistinguishable for CN neurons with different connectivity patterns (Fig. 3b-g)
124 or number of input zones (Supplementary Fig. 4). Thus, we observe that CN neurons with different
125 types of input could not be discerned by their morphological or physiological properties.

126 We next wondered whether the orientation of CN neuron dendrites was related to the location
127 of their Purkinje cell inputs (Supplementary Fig. 5). We found that most cells had at least some
128 dendrites oriented towards their Purkinje cell inputs, but that it was typically a small fraction of
129 the dendritic tree. The amount of dendrite – zone overlap increased as the number of zones
130 connected to a given CN neuron increased, likely due to the greater area covered by the input
131 direction from multiple lobules, suggesting that the orientation of CN dendrites is not shaped by
132 its input. We also did not observe a relationship between IPSC amplitudes or rise times and the
133 degree of overlap, suggesting that dendrites are not preferentially oriented toward or away from
134 larger lobule inputs, and that input from different lobules is not clustered on different regions of
135 the dendritic trees.

136 The CN has previously been described to exhibit a topographic organization that corresponds
137 with the post-synaptic targets of CN neurons[12,21,22]. We wondered whether CN neurons also

138 showed topographic organization according to their input connectivity patterns. Using coordinates
139 from the Allen Mouse Brain Atlas[23], we visualized our recorded cells in 3-D within the fastigial
140 CN[24] (Fig. 4a). CN neurons did not appear to cluster by connectivity pattern (Fig. 4b). However,
141 clustering of CN neurons based on the number of input zones was weakly apparent in our data. To
142 determine whether topographic organization along any axes was observed (Fig. 4c, d), we looked
143 at the fit of cells with different numbers of zonal inputs (e.g., 1 zone, 2 zones, 3 zones, 4 zones,
144 Fig. 4e). We fit a line for each group of cells receiving input from n zones and determined the $R^2$
145 of each. We then performed a bootstrap analysis to randomly sample an equivalent number of cells
146 for each group from our total distribution 50,000 times. To determine how similarly the observed
147 samples' fit matched our data, we assigned significance to any $R^2$ value from our data that was in
148 the top 5% of distribution of bootstrapped $R^2$ values (Supplementary Fig. 6). A significant $R^2$ value
149 was only observed once: for 4 zone cells along the rostroventral-caudodorsal axis (Fig. 4f), but not
150 along the mediolateral axis (Fig. 4g, h). This suggests that 4 zone cells are topographically
151 organized within the fastigial nucleus.
152
153 *Purkinje cell puncta from different zones terminate onto CN neurons in close proximity*
154 Our finding that CN neurons receive Purkinje cell input from multiple cerebellar zones was
155 surprising, so we next validated our findings using a complementary anatomical approach. We
156 performed stereotactic surgeries to inject up to 3 adeno-associated viruses (AAVs) expressing
157 different fluorophores into different cerebellar zones of adult *Pcp2-Cre*-negative mice to label
158 Purkinje cells and their axons. This enabled us to visualize the axons and terminals of Purkinje
159 cells from different locations within the CN (Fig. 5a). We found that Purkinje cells from different
160 zones (Fig. 5b, c) show gross differences in their projection patterns within the nucleus (Fig. 5d),

161 as previously reported[21]. However, in many regions of the CN, we observed puncta from different
162 zones in close proximity (Fig. 5e). In fact, ~30% of puncta from Purkinje cells originating in one
163 zone were located within 17.5 μm of puncta from a different zone, which is the average CN soma
164 diameter (Fig. 5f, Supplementary Fig. 7) and >80% of puncta were located within 97.2 μm, the
165 average length of a CN dendrite (Fig. 5f; Supplementary Fig. 7). This argues that Purkinje cells
166 from different zones frequently terminate within close enough proximity that they can synapse
167 onto the same CN neuron, supporting our optogenetic and electrophysiological findings of
168 convergence across multiple functional zones (Fig. 2).
169
170 *Simultaneous activation of single-zone Purkinje cell inputs is sufficient to silence CN neurons*
171 It has been suggested that Purkinje cell input synchrony is required to affect the output of
172 CN neurons[11]. Our observation that multiple zones converge on single CN neurons raises the
173 question of whether synchrony is required across functional zones to affect cerebellar output. To
174 explore this, we recorded action potentials from CN neurons from spontaneously active cells (Fig.
175 6a, b) prior to breaking through into voltage-clamp configuration for IPSC recordings (Fig. 6c),
176 and stimulated Purkinje cell axons as described above (Fig. 1d). This allowed us to measure both
177 the impact of Purkinje cell stimulation on CN firing and the synaptic response within the same CN
178 neuron. We measured the inter-spike intervals (ISI) of CN neurons immediately after the light
179 pulse as a ratio of the average ISI duration per trial for each CN neuron that fired regularly (Fig.
180 6d, "ISI ratio"). We found that the ISI ratio immediately following stimulation of lobules that were
181 connected to the CN neuron was typically higher than that for lobules that were not synaptically
182 connected to the CN neuron, and the ISI ratio for responsive lobules for each cell after stimulation
183 was greater than the ISI ratio from randomly sampled spike ISIs from the same trial

184 (Supplementary Fig. 8). We found that IPSC amplitude was positively correlated with the ISI ratio
185 (Fig. 6e), where small inputs produced small pauses, and larger inputs produced larger pauses.
186 Remarkably, even small inputs (~60 pA, where ~ 50% of all recorded lobule inputs ≥ 60pA) were
187 sufficient to pause CN firing. Thus, although widespread synchrony across Purkinje cell inputs
188 may occur, our findings suggest that is not necessary since even small inputs can alter CN output.
189

190 **Discussion**

191 Our results reveal how CN neurons in the fastigial nucleus receive input from Purkinje cells
192 that arise from multiple locations across the cerebellar vermis2023-03-17 2:00:00 PM[13,14],
193 revealing that CN neurons are an overlooked locus of cerebellar integration. Using
194 electrophysiology combined with focal optogenetic stimulation of Purkinje cell input, we mapped
195 the spatial patterns of inputs onto CN neurons. We found that input from Purkinje cells tended to
196 recapitulate the transverse zones of the cerebellar cortex, with roughly two thirds of CN neurons
197 receiving uni-zonal input. However, some CN neurons received input from multiple zones. In
198 particular, input from all four functional zones was observed more often than predicted by a
199 random model, and these 4-zone cells appeared to be topographically located near the midline of
200 the rostrodorsal – caudoventral axis in the CN. Corroborating these findings, we used stereotactic
201 viral expression of multiple fluorescent proteins to provide morphological evidence that puncta
202 from Purkinje cells in different functional zones are proximal to puncta from other zones within
203 the CN. Lastly, we showed that small synaptic inputs could pause CN neurons, and that the size
204 of the synaptic response was correlated with the length of the pause. These data demonstrate that
205 widespread Purkinje cell synchrony may not be necessary to influence CN neuron output. Taken

206 together, our results reveal that CN neurons are dynamic computational units that contribute more
207 to cerebellar integration than was previously appreciated.

208 One of the limitations of our study is that connectivity is restricted to axons within the
209 thickness of the slice preparation. While fastigial neurons receive most input from the vermis in a
210 spatially restricted manner[13,14], this suggests that the connectivity patterns we report correspond to
211 a lower limit, and that some multi-zonal cells may have been misclassified as uni-zonal due to
212 missed input. Notably, the size of the dendritic trees did not differ across cells with different
213 numbers of zonal inputs, suggesting that this was not a systematic artifact of slice preparation.
214 Despite our finding that 4-zone connectivity was over-represented, we may nonetheless
215 underestimate the prevalence of these cells in the CN. Furthermore, it is possible that findings in
216 the fastigial nucleus may not resemble the input connectivity patterns in the interposed and dentate
217 nuclei given the distinct three-dimensional features of each nucleus, as well as their different
218 downstream targets[12,14,21,25].

219 Functional transverse zones have been proposed as an underlying feature of the cerebellar
220 cortex based on cerebellar development, different patterns of gene expression, and Purkinje cell
221 physiology[5–10]. Our observation that input to CN neurons clusters based on these zones of the
222 cerebellar cortex underscores the importance of zonal organization in the cerebellum. We observed
223 that CN neurons receiving 4-zone inputs from Purkinje cells were observed more than would be
224 expected from a uniformly random model. Multi-zonal convergence onto a CN neuron suggests a
225 previously unknown site for multimodal integration and output. Such multimodal integration has
226 been observed before at the input level of the cerebellum in the granule cells[26], and is also a feature
227 of Purkinje cells, that integrate large numbers of inputs in their extensive dendritic trees[27–30].
228 However, it has not been clear whether such multimodal integration occurred in the CN. The

229 enrichment of 4-zone input CN neurons in our data suggests that multimodal processing may be a
230 feature of these neurons, and that they function as "integrator neurons" in the cerebellar circuit.

231 Recently a great deal of work has focused on the different classes of neurons of the CN,
232 based on their projections, molecular expression, and physiological properties[12,14,20,31]. We
233 expected that CN neurons might exhibit distinct features based on their input patterns. Our inability
234 to detect any morphological or physiological distinctions does not mean that they do not exist.
235 While properties such as firing rate have been described to differ for different classes of CN
236 neurons, the distributions of firing rates for each category overlaps, meaning that large numbers
237 are needed to differentiate between these cell types[20]. We would be unlikely to discern small
238 differences in overlapping distributions between CN neuron classes because the number of neurons
239 we have characterized in each class is relatively low. However, the topographic enrichment of 4-
240 zone input cells spread along the rostroventral-caudodorsal axis, where 4-zone input cells are
241 tightly clustered in the orthogonal rostrodorsal-caudoventral axis, is likely to have implications for
242 the output circuits of the CN[12,25], although they do not appear to represent any defined output cell
243 population identified to date (e.g. ref.[12]).

244 Several different theories have set out to explain how the cerebellum processes sensorimotor
245 information while producing complex behaviors. In the universal cerebellar transform hypothesis,
246 the cerebellum uses a one-size-fits-all computation to process diverse input and contribute to motor
247 and cognitive functions[32,33]. Alternatively, the multiple functionality transform hypothesis[34] posits
248 that distinct tasks require distinct algorithms which may be mediated by factors such as Purkinje
249 cell firing rate, molecular profile, or timing rules[34–36]. Since neither theory has incorporated a role
250 for CN neurons in cerebellar processing[37], our findings suggest that theories of cerebellar function
251 may need to be updated.

252 Both CN neurons and Purkinje cells fire spontaneous action potentials at high frequencies.
253 If inputs from different Purkinje cells were activated asynchronously, individual inputs may not
254 impact CN output. If, however, Purkinje cell inputs were activated synchronously, the
255 synchronized, stronger inputs may be more able to influence CN output[11]. Interestingly, our data
256 show that even relatively small inputs of ~60 pA can alter CN neuron output, which is smaller than
257 the previously estimated unitary amplitude for Purkinje cell – CN neuron synapses[11]. This suggests
258 that input synchrony from Purkinje cells across different zones may not be strictly necessary,
259 although it does not rule out that it occurs. Purkinje cell synchrony is still possible, since larger
260 amplitude synaptic responses had a stronger impact on CN output. It will be important in the future
261 to determine whether the synchronicity of multi-zonal Purkinje cell input onto individual CN
262 neurons can influence CN neuron output, as this will influence the role of CN information
263 processing in the cerebellum.

264 **Methods**

265 *Animals*

266 We crossed mice hemizygous for Purkinje cell-specific Cre [strain B6.Cg-Tg(Pcp2-
267 cre)3555Jdhu/J; stock number: 010536; PCP2-Cre] with mice with a loxP-flanked stop cassette
268 upstream of Channel-rhodopsin-2(ChR2)/H134R fused with enhanced YFP [strain: B6;129S-
269 Gt(ROSA)26Sor$^{tm32(CAG–COP4*H134R/EYFP)Hze}$/J; stock number 012569; Ai32] to produce hemizygous
270 PCP2-Cre/Ai32 mice [15] that express ChR2 in Purkinje cells, or ChR2(H134R)-EYFP mice. All
271 animal procedures were approved by the McGill Animal Care Committee, in accordance with
272 guidelines established by the Canadian Council on Animal Care.

273

274 *Acute Slice Preparation*

275 Acute sagittal slices were prepared as previously described[38] from 22 female and 25 male mice,
276 aged postnatal day P21 to P32 (Supplementary Fig. 9). Mice were deeply anesthetized with
277 isoflurane until unresponsive to a toe pinch and were then rapidly decapitated. Brains were
278 removed and placed in partial sucrose replacement slicing solution (in mM: 50 NaCl, 2.5 KCl, 0.5
279 $CaCl_2$, 10 $MgCl_2$, 1.25 $NaH_2PO_4$, 25 $NaHCO_3$, 25 glucose, and 111 sucrose bubbled with 95%
280 O2–5% $CO_2$, to maintain pH at 7.3; osmolality ~320 mOsm) heated to ~37º C[39], or in a subset of
281 experiments, in ice-cold slicing solution. We used a Leica VT 1200S vibrating blade microtome
282 (Leica Microsystems, Wetzlar, Germany) to cut parasagittal slices of left cerebellar paravermis at
283 a thickness of 200 µm in a chamber heated to 37º C. Slices were incubated in artificial
284 cerebrospinal fluid (ACSF; in mM: 125 NaCl, 2.5 KCl, 2 $CaCl_2$, 1 $MgCl_2$, 1.25 $NaH_2PO_4$, 25
285 $NaHCO_3$, and 25 glucose, bubbled with carbogen; osmolality ~320 mOsm) at 37°C for 30–45 min
286 in a darkened slice chamber[38], and subsequently moved to room temperature for up to 6 h.
287 Chemicals were purchased from Sigma-Aldrich (Oakville, ON, Canada) except $CaCl_2$ and $MgCl_2$
288 from Fisher Scientific (Toronto, ON, Canada).
289
290 *Electrophysiology*
291 Using acute sagittal slices from mice expressing ChR2 in Purkinje cells, we performed cell-
292 attached and whole-cell patch clamp recordings from CN neurons from the fastigial (medial)
293 cerebellar nucleus. To do this, we pulled borosilicate patch pipettes (2–7 MΩ) using a P-1000
294 puller (Sutter Instruments, Novato, CA, United States) and filled pipettes with an internal solution
295 containing (in mM): 150 potassium gluconate, 3 KCl, 10 HEPES, 0.5 EGTA, 3 Mg-ATP, 0.5 GTP
296 tris salt, 5 phosphocreatine-(di)tris, with 302 mOsm and pH 7.2 (adjusted with KOH). AlexaFluor
297 594 (50 mM, ThermoFisher, Burlington, ON, CA) was added to the internal solution to fill patched

298 CN neurons to enable post-recording imaging and morphological reconstruction. Recordings were
299 acquired with a Multiclamp 700B amplifier (Molecular Devices, Sunnyvale, CA, United States)
300 on a SliceScope Pro 3000 microscope (Scientifica, Uckfield, United Kingdom) from CN neurons
301 in slices maintained at a temperature of 34°C ± 1°C bathed with oxygenated ACSF. For cell-
302 attached recordings, we recorded from spontaneously-firing CN neurons before breaking through
303 into whole-cell patch configuration. For voltage-clamp recordings, CN neurons were clamped at
304 −60 mV and $R_{in}$ and resting membrane potential were monitored, and recordings were excluded if
305 $R_{in}$ fluctuated more than 20%. Data acquisition was performed using custom IGOR Pro acquisition
306 software[38,40] (Wavemetrics, Portland, OR, United States).
307
308 *Optogenetics and spatial mapping*
309 We used a Polygon400E patterned spatial illuminator with a 470 nm LED light source (Mightex,
310 Toronto, ON, Canada) at an estimated focal plane power density of 100 mW/mm$^2$ through a 40X
311 water-immersion objective (Olympus LUMPLFLN40XW, Tokyo, Japan) to optically stimulate
312 Purkinje cell axons focally[38] using a blue rectangular (85 x 95 μm) light pulse of 3 ms with an
313 inter-trial interval of 10 ms. To assess cell health, we stimulated the patched CN neuron to activate
314 a large proportion of the synaptic inputs onto the cell directly (Purkinje cell "axonal terminals").
315 We next stimulated the base of each lobule sequentially (e.g. moving from lobule II to III to IV/V,
316 etc. to lobule X, then over the axonal terminals, for ≥ 3 trials per location to identify functionally
317 connected lobules. In a subset of CN neurons, we sampled connectivity by stimulating Purkinje
318 cell axons at additional locations.
319 To assess the impact of synaptic input on CN neuron spontaneous firing, we performed cell-
320 attached recordings in CN neurons and sequentially stimulated individual lobules as described

321 above before breaking through into voltage-clamp mode. We excluded cells that broke through
322 into whole-cell mode before stimulating each lobule at least once, trials in which spontaneous
323 firing frequency was < 20 Hz, and trials that were marked by bursting rather than tonic firing. After
324 completing the stimulation protocol in cell-attached mode, we broke through and patch-clamped
325 the CN neurons to compare voltage-clamp recorded IPSCs with their corresponding spontaneous
326 firing data.
327
328 *Analysis of electrophysiological data*
329 All electrophysiological data were analyzed using custom Igor Pro data analysis software[38,40]. For
330 IPSCs, the rise time was measured as the time between 20-80% of the peak (standard deviation,
331 SD)[38]. To assess the decay phases of synaptic currents, we used a double-exponential to fit the
332 decay phases of IPSCs and calculated weighted decay τ time constants by assessing the
333 contribution of each component of the exponential to the peak IPSC amplitude[16]. Proportion of
334 failures was measured as the number of trials in which a responsive lobule failed to elicit an IPSC
335 while the patch was still successfully in place as determined by the axonal terminal stimulation.
336 For CN neurons that received input from more than one lobule or zone, we compared differences
337 in amplitudes and rise times between individual IPSCs using a disparity index, or a measure of the
338 coefficient of the variation of evoked IPSC amplitudes[17].
339
340 *Identifying connectivity motifs*
341 To determine whether structure in connectivity patterns was observed, we performed two analyses.
342 First, we created a binary dataset including each CN neuron's connectivity to lobules III through
343 X, excluding lobule II since several lateral slices did not include lobule II, and excluding neurons

344 from which we did not identify a connected lobule (n = 34 cells). We then performed unsupervised
345 hierarchical clustering of the cells with identified functional connections (n = 41 cells). We used
346 Seaborn to create a clustergram of the binary connections between cells (Fig. 2b, rows) and lobules
347 (Fig. 2b, columns) based on the Hamming distances between lobules with an unweighted average
348 linkage. Input from lobules II, III, and/or IV/V were categorized as the anterior zone; lobule VI/VII
349 as the central zone; lobule VIII, IX (without lobule X) as the posterior zone; input from lobule IX
350 and X, or only lobule X, as the nodular zone.
351 To identify whether a given pattern of input to a CN neuron constituted a motif, or a statistically
352 overrepresented connectivity pattern in our dataset, we tested the following hypothesis. From
353 adequately sampled CN neurons, we assumed input from each of the four cerebellar zones to occur
354 independently of input from another zone. We calculated the probability of input from each zone
355 within the dataset independent of each other probability. To evaluate multi-zone connectivity
356 patterns, we multiplied the probability of each zone occurring in our dataset to the probability of
357 the other combination(s), multiplied by the probably of non-connection to excluded zones. For
358 example, a Central-Posterior input probability = the probability of input from the central zone (26
359 cells/75 cells tested) * the probability of input from the posterior zone (16 cells/75 cells tested) *
360 by the probability of not-A anterior zone (1 – 13/75 cells) * the probability of not-N nodular zone
361 (1 – 13/75 cells) = (0.347 * 0.213 * 0.827 * 0.827). We then compared the actual probability of
362 the combinations occurring in our dataset to the predicted using a binomial probability test, where
363 combinations that occurred significantly more or less often than predicted were described as
364 "motifs."
365
366 *Intracranial viral surgeries*

367 To label Purkinje cell axonal projections to CN neurons, we first injected *Pcp2*-Cre negative mice
368 intraperitoneally with a 25% solution of mannitol in PBS (7.5g/Kg; Sigma-Aldrich, Oakville, ON,
369 Canada) in order to enhance virus distribution[41,42]. Mice were then anesthetized using isoflurane
370 (2.5% mixture in O2) before their fur was shaved and they were transferred to a stereotactic frame
371 (Stoelting Co). Carprofen was given subcutaneously, and a lidocaine/bupivacaine mixture was
372 applied locally for analgesia. We performed three injections on each mouse from posterior to
373 anterior. Under stereotactic guidance, a small craniotomy was drilled (< 1 mm) at the first location
374 using a dental drill. A capillary filled with mineral oil (Sigma-Aldrich, Oakville, ON, Canada)
375 attached to a nanoinjector (WPI, Sarasota, Florida, USA) was filled with 150-250 nL of virus,
376 injected into the posterior cerebellar vermis (lobule VIII) and allowed to diffuse for five minutes.
377 Once retracted, the mineral oil-filled capillary was replaced and realigned with Bregma. The
378 second and third injections were performed in the central (lobule VI/VII) and anterior vermis
379 (lobule IV/V) as described. The injection coordinates for surgeries were as follows along the
380 midline ($X$=0) from Bregma ($Y, Z$): Posterior vermis: (-7.25, -4.0 or 7.25, -4.25); Central vermis (-
381 6.9, -2.5 or -6.9, -1.8 or -6.65, -1.8); Anterior vermis (-5.65, -3.0 or -5.7, -2.0 or -5.85, -2.5). We
382 used the following viruses to label Purkinje cell axons arising from different cerebellar zones:
383 pENN.AAV.CB7.CI.mCerulean.WPRE.RBG (titer $\geq 5\times10^{12}$ vg/mL), pAAV-CAG-tdTomato
384 (codon diversified; titer $\geq 1\times10^{13}$ vg/mL) and pAAV-CAG-GFP (titer $\geq 7\times10^{12}$ vg/mL) viral preps
385 were purchased from Addgene (Addegene viral prep #: 105557-AAV9, 59462-AAV8 and 37825-
386 AAV8). After surgeries, mice were allowed to recover for 2-3 weeks before being euthanized and
387 perfused as described below.
388
389 *Immunohistochemistry and viral labeling*

390 We performed immunohistochemistry to demonstrate that CN neurons do not express ChR2 by
391 perfusing mice and labeling for NeuN and anti-green fluorescent protein (GFP). For both
392 immunohistochemistry and viral labeling experiments, we prepared slices from animals by deeply
393 anesthetizing mice with 2,2,2-tribromoethanol (avertin, 0.02 mL/10g) via intraperitoneal injection,
394 followed by intracardiac perfusion[43]. We performed an initial flush using PBS and 5.6 μg/ml
395 heparin salt, followed by perfusion with 40 ml of 4% PFA in phosphate buffer (PB, pH 7.4). We
396 stored brains in 4% PFA for two days at 4ºC on a shaker at 70 RPM, followed by storage in PBS
397 with 0.5% sodium azide prior to slicing. We collected sagittal slices (100 μm thickness) using a
398 Vibratome 3000 sectioning system (Concord, ON, Canada). To label slices with NeuN and anti-
399 GFP, we incubated slices for thirty minutes in blocking solution (1x PBS, 0.1M, pH 7.4; 0.4%
400 Triton X; 5% bovine serum albumin (BSA); and 0.05% sodium azide) which was followed by a
401 3-day incubation with the primary antibodies in blocking solution. During primary antibody
402 incubation, CN neurons were labeled with guinea pig anti-NeuN primary antibody (1:500, abN90,
403 Millipore, Burlington, MA, United States) and rabbit anti-GFP primary antibody (1:500, ab3080,
404 Millipore, Burlington, MA, United States). Slices were subsequently labeled with DyLight 405
405 anti-guinea pig secondary antibody (1:500, 106475003, Jackson Immunoresearch) and goat Alexa
406 594 anti-rabbit secondary antibody (1:1000, A11037, Life Technologies) during a 90-minute
407 incubation in blocking solution. We then rinsed and immediately mounted slices onto glass slides
408 with Prolong Gold Antifade (ThermoFisher Scientific, Waltham, MA, United States) under low
409 light, then stored slides in the dark at 4°C.
410
411 *Image acquisition and analysis*

412 Immediately after electrophysiology experiments, we performed live two-photon imaging of
413 AlexaFluor 594-filled CN neurons on a custom-built two-photon microscope (Scientifica) imaged
414 with a Ti:Sapphire laser (MaiTai; Spectra Physics, Santa Clara. CA, USA) tuned to 890 nm, as
415 previously described[44]. Images were acquired at a resolution of 512 by 512 pixels using ScanImage
416 3.7 running in MatLab 2011B (Mathworks, Natick, MA, USA). We later re-imaged slices
417 containing filled CN neurons using a LSM800 laser scanning confocal microscope at 10x and 20x
418 using Zeiss Zen software (Zeiss, Oberkochen, Germany) following immunohistochemistry
419 staining and fixation in 4% paraformaldehyde (PFA). Slices labeling Purkinje cell puncta (anti-
420 GFP) onto CN neurons (anti-NeuN) were imaged using the same confocal microscope.
421 After imaging prepared slices, we used Fiji (ImageJ, NIH)[45] to analyze filled, stained CN neurons
422 from electrophysiology and immunohistochemistry experiments. We confirmed the identity of
423 AlexaFluor 594-filled CN neurons by comparing them with the initial two-photon images acquired
424 following live electrophysiology experiments and identified the dendritic and lobule orientation in
425 slices with filled cells to evaluate the relationship between CN morphology and input patterns. We
426 used Neurolucida software (MBF Biosciences, Williston, VT, USA) to manually perform
427 morphological reconstructions of CN neurons from the two-photon imaging session following
428 patch clamp experiments. We traced cells in 3-D to obtain the cell soma contours, dendrite
429 projections, and axon within the image stack. We imported tracings into Neurolucida Explorer to
430 extract morphological data, including soma area, soma diameter, number, and length of dendrites.
431 Branch index was calculated by dividing the number of dendritic crossings 25 μm from the cell
432 soma by the number of primary dendrites[20]. Polar plots were made using IgorPro to evaluate the
433 overlap between dendritic orientation and Purkinje cell input. Dendritic polar plots were
434 normalized to the length of the longest dendrite.

435 To evaluate the proximity of virally-labeled Purkinje cell puncta originating from different
436 cerebellar zones following intracranial stereotactic surgeries, we imaged mounted 100 µm-thick
437 sections using the LSM-800 confocal microscope at 10x, 20x, and 63x oil immersion and acquired
438 tiled stacks. We used ImageJ to identify the X and Y coordinates of each puncta of each fluorescent
439 color. Using a custom Python script, we identified the nearest neighbor puncta across different
440 zonal inputs with different imaging channels to identify the Euclidean distance of the nearest
441 puncta across zones. To confirm that there was little to no colocalization of multiple viruses in the
442 same Purkinje cells, we performed thresholding of Purkinje cell puncta for each channel in ImageJ
443 and acquired the positions of puncta in the X-Y plane using ImageJ's plot profile analysis function
444 and used a custom Python script to identify the percentage of colocalized pixels per slice in each
445 stack which determined there was virtually no colocalization between channels (Table S1).
446
447 *Cell topography within fastigial nucleus*
448 The position of each recorded CN neuron (Fig. 5) was recorded manually during each experiment
449 and paired with an image of the position of each patch pipette during the recording. We mapped
450 these positions for each slice along the mediolateral axis using the coordinate system from the
451 Allen Mouse Brain Atlas[23], and for cells that were successfully filled with Alexa594 during each
452 experiment, we confirmed these positions after confocal imaging of each slice. We then used
453 Brainrender[24] to visualize these cells in 3-D within the nucleus. Next, we represented plotted CN
454 neurons based on their number of input zones (0 to 4 zones) along the Allen Mouse Brain Atlas
455 coordinates and produced graphs along the rostro-caudal and ventral-dorsal axes. We performed a
456 linear regression for each category (n = 0, 1, 2, 3, or 4 zones) and identified the $R^2$ value for each
457 group. To evaluate whether the strength of the best fit line for each category was significant, we

458 performed a bootstrap analysis where we randomly sampled n cells (equivalent to the number of
459 cells in our dataset that received input from n zones) from each category 50,000 times and
460 determined whether the $R^2$ value from our data occurred within the top 5% of $R^2$ values from the
461 bootstrapped samples. We plotted the percentile of the $R^2$ values from our data compared to the
462 bootstrapped samples as the "probability of $R^2$ compared to 50,000 random samples" (Fig. 4f, g).
463

464 *Statistics*

465 We used JMP software (SAS, Carey, NC, United States), to perform Student's t-tests on datasets
466 with normal distributions, and Igor Pro software for non-parametric Mann–Whitney *U* tests for
467 datasets with non-normal distributions, with the level of significance (α) set at $P < 0.05$. To
468 evaluate connectivity motifs, we used a binomial distribution calculator followed by multiple
469 hypothesis corrections using the Benjamini-Hochberg method. Data are reported as mean ± SEM
470 unless otherwise indicated. For all data, *n* = number of neurons and *N* = number of mice.
471

472 **Acknowledgements**

473 We thank D. Bowie, J. Lefebvre, and T. Ohyama for helpful advice. We thank C. Chou for training
474 and technical support. We thank C. Vaaga, N. Al-Sharif, and J.W. Vogel for advice about data
475 analysis. We thank all current and former members of the Watt laboratory for advice and support,
476 especially S. Jayabal and D. Lang-Ouellette. We thank the staff at the Advanced BioImaging
477 Facility (ABIF) at McGill University for their technical support with confocal imaging. We thank
478 A. Hargreaves and students from BIOL 610 at McGill for helpful comments and support in drafting
479 an early version of this manuscript. We thank T. Koch and the other team members from the
480 Comparative Medicine and Animal Resources Centre (CMARC) for their technical support.

## Funding

This work was supported by the following: NSERC Discovery grants (RPGIN-2016005118 and RGPIN-2022-03439) and CIHR project grant (PJT-153150) (A.J.W.), a Fonds de recherche du Québec – Nature et technologies (FRQNT) Doctoral Scholarship, a McGill Integrated Program in Neuroscience Graduate Excellence Award, and a Graduate Student Fellowship from the Canada First Research Excellence Fund Healthy Brains for Healthy Lives initiative (K.M.G.), and a Fonds de recherche du Québec – Santé (FRQS) Doctoral Scholarship (E.F.).

## Author Contributions

K.M.G. designed and ran experiments for all figures except Fig. 5, analyzed data for all figures, and wrote the manuscript.; J.W.Y.J. analyzed data for Figs. 3-4, S4-5, and S7.; E.F. designed and ran experiments for Fig. 5; S.S. analyzed data for Fig. 2; P.J.S. wrote custom Igor software packages for electrophysiology data acquisition and analysis, and analyzed data for Figs. 2 and 4. A.J.W. conceived of the project, designed experiments, analyzed data, supervised the project, and wrote the manuscript.

## Competing Interests

The authors declare that they have no competing interests.

501 **References**


502 1. King, M., Hernandez-Castillo, C. R., Poldrack, R. A., Ivry, R. B. & Diedrichsen, J. Functional
503 boundaries in the human cerebellum revealed by a multi-domain task battery. *Nature*
504 *Neuroscience* **22**, 1371–1378 (2019).
505 2. Larivière, R. *et al.* Sacs knockout mice present pathophysiological defects underlying
506 autosomal recessive spastic ataxia of charlevoix-saguenay. *Human Molecular Genetics* **24**,
507 727–739 (2015).
508 3. Stoodley, C. J. *et al.* Altered cerebellar connectivity in autism and cerebellar-mediated rescue
509 of autism-related behaviors in mice. *Nat Neurosci* **20**, 1744–1751 (2017).
510 4. Kelly, E. *et al.* Regulation of autism-relevant behaviors by cerebellar–prefrontal cortical
511 circuits. *Nat Neurosci* **23**, 1102–1110 (2020).
512 5. Apps, R. & Hawkes, R. Cerebellar cortical organization: a one-map hypothesis. *Nature*
513 *Reviews Neuroscience* **10**, 670–681 (2009).
514 6. Reeber, S. L., White, J. J., George-Jones, N. A. & Sillitoe, R. V. Architecture and development
515 of olivocerebellar circuit topography. *Frontiers in Neural Circuits* **0**, 115 (2012).
516 7. Ozol, K., Hayden, J. M., Oberdick, J. & Hawkes, R. Transverse zones in the vermis of the
517 mouse cerebellum. *Journal of Comparative Neurology* **412**, 95–111 (1999).
518 8. Apps, R. *et al.* Cerebellar Modules and Their Role as Operational Cerebellar Processing Units.
519 *Cerebellum* **17**, 654–682 (2018).
520 9. Zhou, H. *et al.* Cerebellar modules operate at different frequencies. *eLife* **2014**, 1–18 (2014).
521 10. Zhou, H., Voges, K., Lin, Z., Ju, C. & Schonewille, M. Differential Purkinje cell simple spike
522 activity and pausing behavior related to cerebellar modules. *Journal of Neurophysiology* **113**,
523 2524–2536 (2015).

524 11. Person, A. L. & Raman, I. M. Purkinje neuron synchrony elicits time-locked spiking in the
525 cerebellar nuclei. *Nature* **481**, 502–505 (2012).
526 12. Fujita, H., Kodama, T. & du Lac, S. Modular output circuits of the fastigial nucleus for diverse
527 motor and nonmotor functions of the cerebellar vermis. *eLife* **9**, e58613 (2020).
528 13. Gould, B. B. The organization of afferents to the cerebellar cortex in the cat: Projections from
529 the deep cerebellar nuclei. *Journal of Comparative Neurology* **184**, 27–42 (1979).
530 14. Kebschull, J. M. *et al.* Cerebellar nuclei evolved by repeatedly duplicating a conserved cell-
531 type set. *Science* **370**, (2021).
532 15. Jackman, S. L., Beneduce, B. M., Drew, I. R. & Regehr, W. G. Achieving High-Frequency
533 Optical Control of Synaptic Transmission. *Journal of Neuroscience* **34**, 7704–7714 (2014).
534 16. Vaaga, C. E., Brown, S. T. & Raman, I. M. Cerebellar modulation of synaptic input to freezing-
535 related neurons in the periaqueductal gray. *eLife* **9**, (2020).
536 17. Hashimoto, K. & Kano, M. Functional Differentiation of Multiple Climbing Fiber Inputs
537 during Synapse Elimination in the Developing Cerebellum. *Neuron* **38**, 785–796 (2003).
538 18. Song, S., Sjostrom, P. J., Reigl, M., Nelson, S. & Chklovskii, D. B. Highly nonrandom features
539 of synaptic connectivity in local cortical circuits. *PLoS Biology* **3**, 0507–0519 (2005).
540 19. Rieubland, S., Roth, A. & Häusser, M. Structured connectivity in cerebellar inhibitory
541 networks. *Neuron* **81**, 913–929 (2014).
542 20. Uusisaari, M., Obata, K. & Knöpfel, T. Morphological and electrophysiological properties of
543 GABAergic and non-GABAergic cells in the deep cerebellar nuclei. *Journal of*
544 *neurophysiology* **97**, 901–11 (2007).

21. Sugihara, I. *et al.* Projection of reconstructed single Purkinje cell axons in relation to the cortical and nuclear aldolase C compartments of the rat cerebellum. *Journal of Comparative Neurology* **512**, 282–304 (2009).

22. Sugihara, I. & Shinoda, Y. Molecular, Topographic, and Functional Organization of the Cerebellar Nuclei: Analysis by Three-Dimensional Mapping of the Olivonuclear Projection and Aldolase C Labeling. *Journal of Neuroscience* **27**, 9696–9710 (2007).

23. Wang, Q. *et al.* The Allen Mouse Brain Common Coordinate Framework: A 3D Reference Atlas. *Cell* **181**, 936-953.e20 (2020).

24. Claudi, F. *et al.* Visualizing anatomically registered data with brainrender. *eLife* **10**, e65751 (2021).

25. Sugihara, I. Compartmentalization of the deep cerebellar nuclei based on afferent projections and aldolase C expression. *Cerebellum* **10**, 449–463 (2011).

26. Ishikawa, T., Shimuta, M. & Häuser, M. Multimodal sensory integration in single cerebellar granule cells in vivo. *eLife* **4**, (2015).

27. Kitamura, K. & Häusser, M. Dendritic Calcium Signaling Triggered by Spontaneous and Sensory-Evoked Climbing Fiber Input to Cerebellar Purkinje Cells In Vivo. *J Neurosci* **31**, 10847–10858 (2011).

28. Pijpers, A., Apps, R., Pardoe, J., Voogd, J. & Ruigrok, T. J. H. Precise Spatial Relationships between Mossy Fibers and Climbing Fibers in Rat Cerebellar Cortical Zones. *J. Neurosci.* **26**, 12067–12080 (2006).

29. Roome, C. J. & Kuhn, B. Dendritic coincidence detection in Purkinje neurons of awake mice. *eLife* **9**, e59619 (2020).

567 30. Wang, S. S.-H., Denk, W. & Häusser, M. Coincidence detection in single dendritic spines
568 mediated by calcium release. *Nat Neurosci* **3**, 1266–1273 (2000).
569 31. Novello, M., Bosman, L. W. J. & De Zeeuw, C. I. A Systematic Review of Direct Outputs
570 from the Cerebellum to the Brainstem and Diencephalon in Mammals. *Cerebellum* (2022)
571 doi:10.1007/s12311-022-01499-w.
572 32. Schmahmann, J. D. The role of the cerebellum in affect and psychosis. *Journal of*
573 *Neurolinguistics* **13**, 189–214 (2000).
574 33. Schmahmann, J. D., Guell, X., Stoodley, C. J. & Halko, M. A. The Theory and Neuroscience
575 of Cerebellar Cognition. *Annual Review of Neuroscience* **42**, 337–364 (2019).
576 34. Diedrichsen, J., King, M., Hernandez-Castillo, C., Sereno, M. & Ivry, R. B. Universal
577 Transform or Multiple Functionality? Understanding the Contribution of the Human
578 Cerebellum across Task Domains. *Neuron* **102**, 918–928 (2019).
579 35. Cerminara, N. L., Lang, E. J., Sillitoe, R. V. & Apps, R. Redefining the cerebellar cortex as an
580 assembly of non-uniform Purkinje cell microcircuits. *Nat Rev Neurosci* **16**, 79–93 (2015).
581 36. Suvrathan, A., Payne, H. L. & Raymond, J. L. Timing Rules for Synaptic Plasticity Matched
582 to Behavioral Function. *Neuron* **92**, 959–967 (2016).
583 37. Kebschull, J. M. *et al.* Cerebellum Lecture: the Cerebellar Nuclei—Core of the Cerebellum.
584 *Cerebellum* (2023) doi:10.1007/s12311-022-01506-0.
585 38. Gruver, K. M. & Watt, A. J. Optimizing Optogenetic Activation of Purkinje Cell Axons to
586 Investigate the Purkinje Cell – DCN Synapse. *Frontiers in Synaptic Neuroscience* **11**, 1–8
587 (2019).
588 39. Ankri, L., Yarom, Y. & Uusisaari, M. Y. Slice it hot: acute adult brain slicing in physiological
589 temperature. *Journal of visualized experiments : JoVE* e52068 (2014) doi:10.3791/52068.

590 40. Watt, A. J. *et al.* Traveling waves in developing cerebellar cortex mediated by asymmetrical
591 Purkinje cell connectivity. *Nature Neuroscience* **12**, 463–473 (2009).
592 41. Carty, N. *et al.* Convection-enhanced delivery and systemic mannitol increase gene product
593 distribution of AAV vectors 5, 8, and 9 and increase gene product in the adult mouse brain.
594 *Journal of neuroscience methods* **194**, 144—153 (2010).
595 42. Mastakov, M. Y., Baer, K., Xu, R., Fitzsimons, H. & During, M. J. Combined Injection of
596 rAAV with Mannitol Enhances Gene Expression in the Rat Brain. *Molecular Therapy* **3**, 225–
597 232 (2001).
598 43. Cook, A. A. *et al.* Activation of TrkB-Akt signaling rescues deficits in a mouse model of
599 SCA6. *Science Advances* **8**, eabh3260 (2022).
600 44. Lang-Ouellette, D. *et al.* Purkinje cell axonal swellings enhance action potential fidelity and
601 cerebellar function. *Nature Communications* **12**, 4129 (2021).
602 45. Schindelin, J. *et al.* Fiji: an open-source platform for biological-image analysis. *Nat Methods*
603 **9**, 676–682 (2012).
604

## Figures

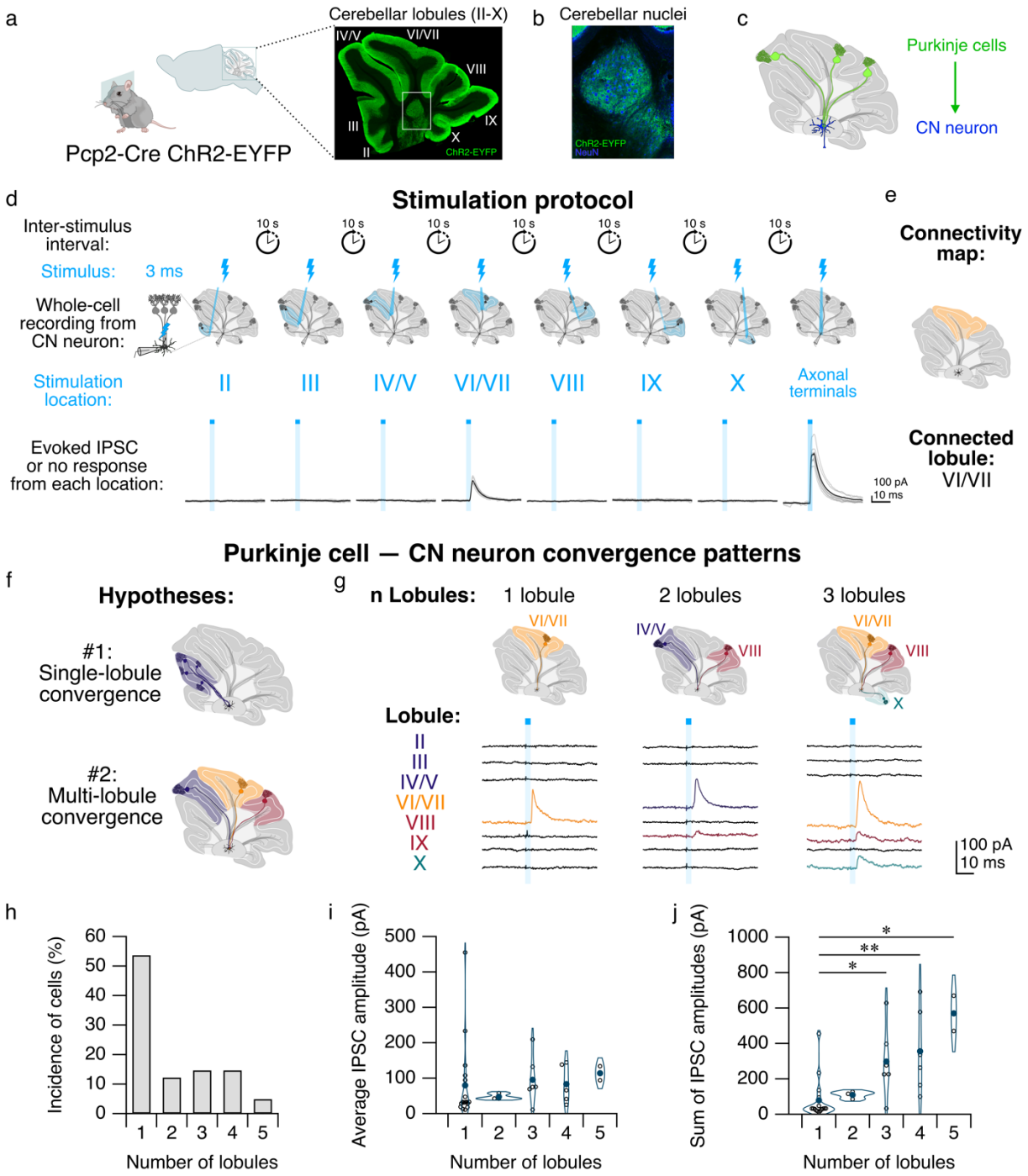


**Figure 1**: Cerebellar nuclear (CN) neurons receive both single-lobule and multi-lobule input. **a**, Left, cartoon of a transgenic mouse expressing Channelrhodopsin-2 (ChR2) fused with enhanced

yellow fluorescent protein (EYFP) in Purkinje cells. Right, ChR2-EYFP (green) in Purkinje cells, with cerebellar lobule divisions. **b**, Expansion of white box in **a** shows ChR2-EYFP expression is restricted to Purkinje cell puncta (green) in the CN, while CN neurons express NeuN (blue). **c**, Purkinje cells predominantly project unidirectionally to CN neurons. **d**, Stimulation protocol. Top, durations of inter-stimulus interval and stimulus. Blue lightning bolts indicate a single 3 ms flash of 470 nm blue light above stimulation location from a focal spatial illuminator via a light-emitting diode. Middle, CN neurons were patch-clamped while Purkinje cell axons in each area (left, base of individual cerebellar lobules II through X; right, axonal terminals) were stimulated in rapid succession. Blue lobule indicates stimulation of Purkinje cell axons within each lobule that are located within the acute slice plane. Bottom, the evoked IPSC was recorded following stimulation. Grey traces represent individual IPSCs, and black traces indicate average. Blue rectangles indicate onset and duration of light pulse. Lobule average IPSC: 99.85 ± 10.65 pA; axonal terminals average IPSC: 402.20 ± 55.13 pA. **e**, Connectivity map representing Purkinje cell – CN connectivity from cell shown in **d**. **f**, Representation of two hypotheses of Purkinje cell convergence on CN neurons. Top, Purkinje cells originating from a single lobule converge on a CN neuron (hypothesis #1); bottom, Purkinje cells originating from multiple lobules converge on a CN neuron (hypothesis #2). **g**, Connectivity maps (top) and average evoked IPSCs (bottom) from three CN neurons receiving input from 1 (left), 2 (middle), or 3 (right) lobules. **h**, Percentage of cells connected to n lobules. **i**, Average IPSC amplitude per cell with n connected lobules. **j**, Sum of IPSC amplitudes per cell with n connected lobules. IPSC amplitudes compared using non-parametric multiple comparison Mann-Whitney $U$ test. $^{*}P < 0.05$, $^{**}P < 0.01$. Unlabeled comparisons = not significantly different.

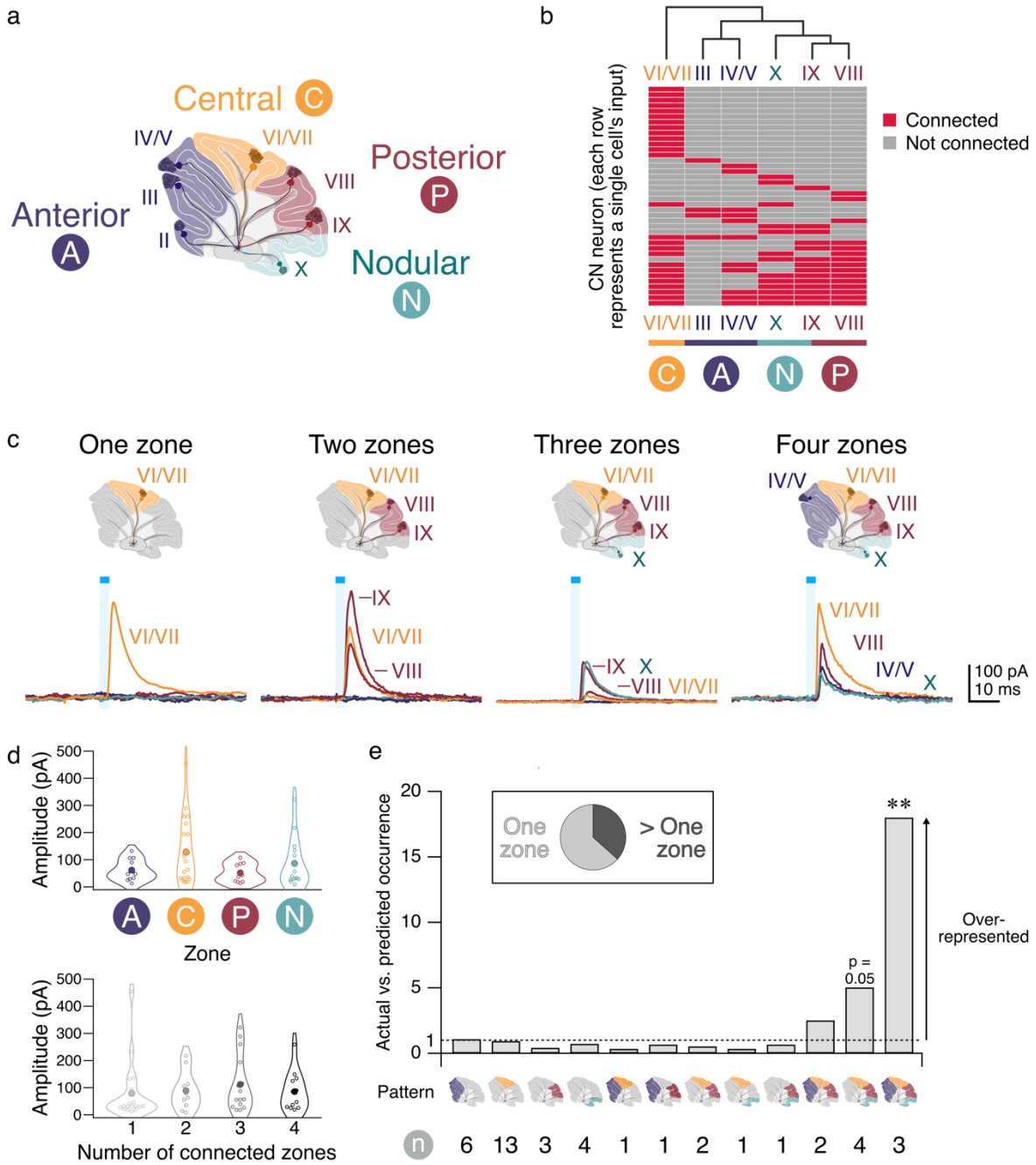


**Figure 2**: Purkinje cell – CN neuron connectivity is not random. **a**, Cartoon of cerebellar lobules (roman numerals) and zones (circles). **b**, Heatmap representing lobule inputs (columns) to individual CN neurons (rows) displaying connected lobules (red) and unconnected lobules (grey). Dendrogram of lobules created with unsupervised hierarchical clustering (top) using the Hamming

distances between lobules' connectivity patterns with the unweighted average linkage reveals inputs cluster along functional zones (delineated by colour, bottom). **c**, Connectivity maps (top) and evoked IPSCs (bottom) from four CN neurons receiving input from one (left), two (middle left), three (middle right), and four (right) zones. Roman numerals beside traces indicate responsive lobule. **d**, Top, average IPSC amplitude for each zone is not statistically different from other zones. Bottom, average IPSC amplitude per cell based on number of connected zones. **e**, Comparison of the actual vs. predicted occurrence of cells with each zone combination found in our dataset. Dotted line represents equal occurrence of predicted and actual combinations. *P* values represent the difference between the actual and predicted occurrence as determined using a binomial distribution test, with multiple hypothesis corrections performed using False Discovery Rate testing. Inset shows proportion of CN neurons receiving input from one zone or multiple zones. IPSC amplitudes compared using non-parametric multiple comparison Mann-Whitney *U* test. $^{**}P < 0.01$. Unlabeled comparisons = not significantly different. n = 41 cells with functional connections out of 75 cells.

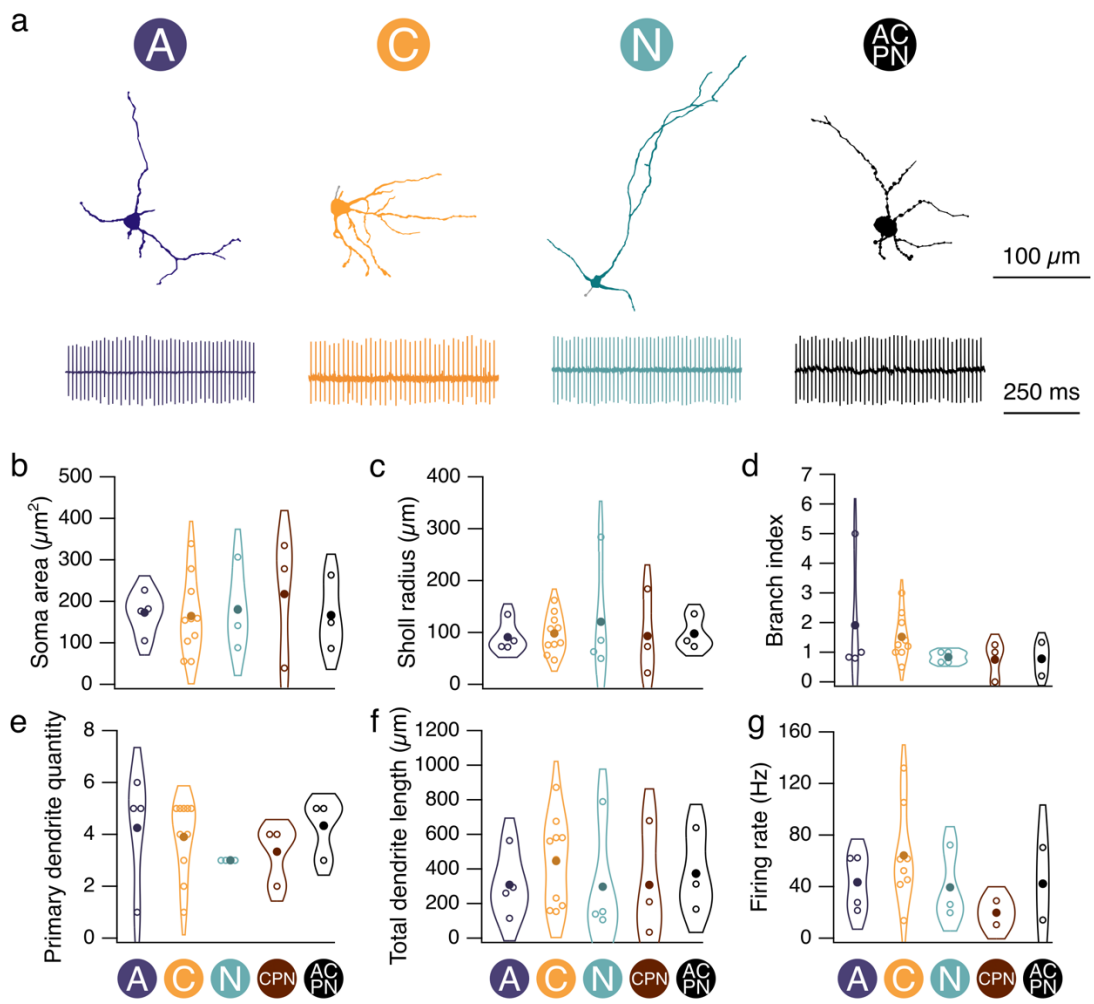


**Figure 3**: CN neurons with different input connectivity patterns are morphologically similar. **a**, Top, reconstruction of CN neurons from two-photon stack. Circle denotes cell receives input from the anterior ("A") zone. Bottom, representative traces of spontaneous firing from CN neurons receiving input from the "A," "C," "N," or "ACPN," zones, respectively, obtained before breaking through into whole-cell configuration. **b-g**, Soma area, Sholl radius, branch index, primary dendrite quantity, total dendrite length, and firing rate for cells with different connectivity patterns, groups with < 3 reconstructed cells were excluded. Morphological properties compared across connectivity patterns using non-parametric multiple comparison Mann-Whitney *U* test. Unlabeled comparisons = not significantly different.

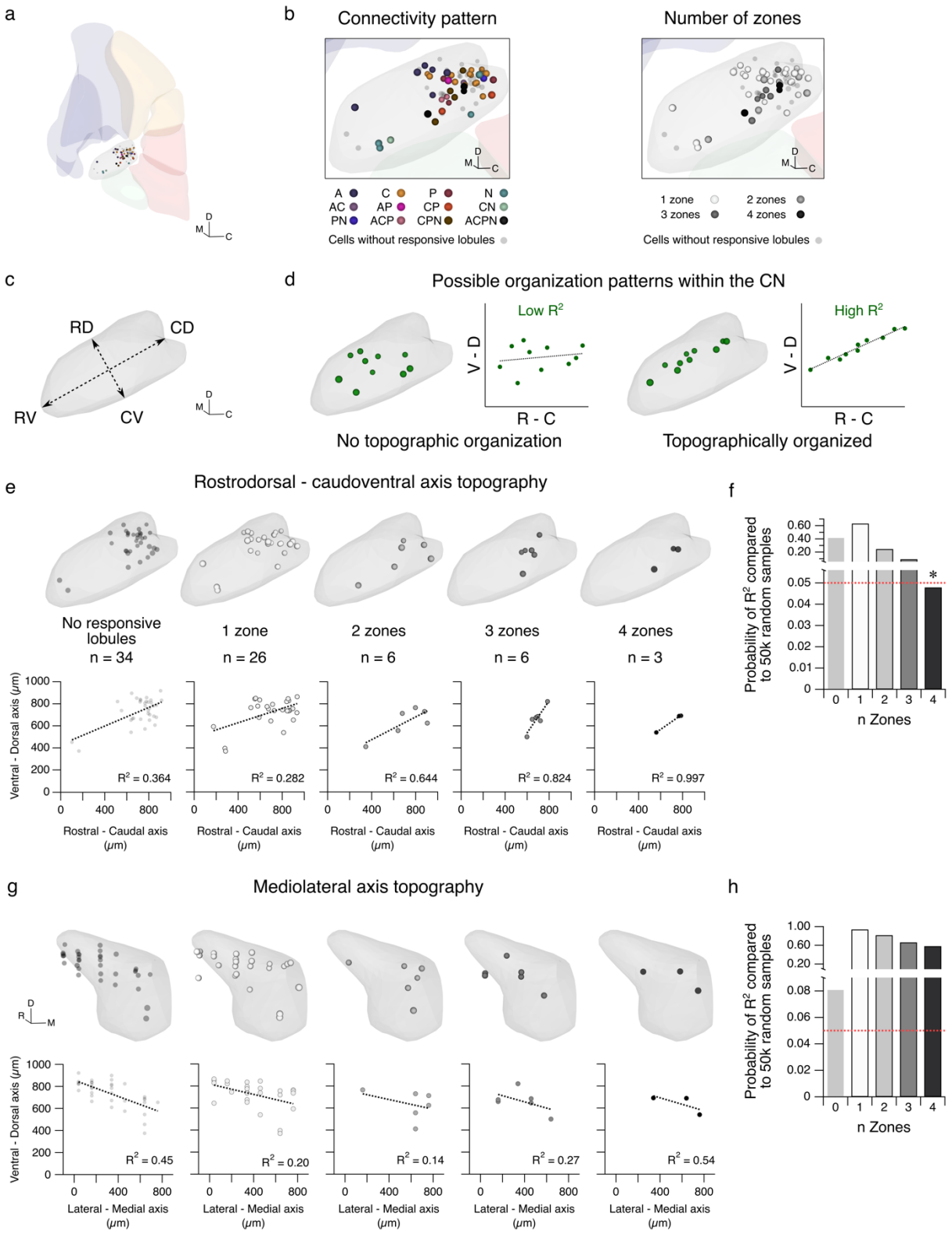
a
D
M
C
b
Connectivity pattern
A
C
P
N
AC
AP
CP
CN
PN
ACP
CPN
ACPN
Cells without responsive lobules
Number of zones
1 zone
2 zones
3 zones
4 zones
Cells without responsive lobules
c
RD
CD
RV
CV
d
Possible organization patterns within the CN
Low R2
High R2
V - D
R - C
No topographic organization
Topographically organized
e
Rostrodorsal - caudoventral axis topography
No responsive lobules
n = 34
1 zone
n = 26
2 zones
n = 6
3 zones
n = 6
4 zones
n = 3
Ventral - Dorsal axis (μm)
Rostral - Caudal axis (μm)
R2 = 0.364
R2 = 0.282
R2 = 0.644
R2 = 0.824
R2 = 0.997
f
Probability of R2 compared to 50k random samples
n Zones
*
g
Mediolateral axis topography
R
M
Ventral - Dorsal axis (μm)
Lateral - Medial axis (μm)
R2 = 0.45
R2 = 0.20
R2 = 0.14
R2 = 0.27
R2 = 0.54
h
Probability of R2 compared to 50k random samples
n Zones

**Figure 4**: CN neurons receiving input from all four zones are biased along the rostroventral-caudodorsal axis. **a**, 3-D representation of recorded cells using coordinates from the Allen Mouse Brain atlas and rendered using Brainrender. **b**, Left, expansion of inset in **a** depicting position of cells based on connectivity pattern. Right, cells in **b, left** categorized by number of input zones. **c,** Rendering of fastigial CN depicting the rostroventral-caudodorsal (RV-CD) and rostrodorsal-caudoventral (RD-CV) axes. **d**, Cartoons of two possible organization patterns within the CN, where one type of CN neurons receiving a pattern of Purkinje cell input do not demonstrate topographic organization (left, "Low $R^2$"), and another where CN neurons receiving a particular pattern of Purkinje cell input exhibit topographic organization biased along a particular axis of the nucleus (right, "High $R^2$"). **e**, Top (from left to right), rendering of position in the sagittal plane of CN neurons that responded only to axonal terminal stimulation (No responsive lobules), and CN neurons that received input from one zone, two zones, three zones, and four zones. Bottom, same as in **e**, **top**, but showing the plotted points for each CN neuron in the rostral-caudal and ventral-dorsal axes. Dotted lines and $R^2$ values in each graph represent the line of best fit for the neurons in each category. **f**, Graph demonstrating the probability that n randomly selected cells from a bootstrapped analysis with 50,000 iterations has an $R^2$ value ≥ the $R^2$ value from each group of n Zones from **e, bottom**. Only the n Zones = 4 group demonstrates an $R^2$ value ≥ 0.997 in fewer than 5% of the bootstrapped samples. Red dotted line indicates $P = 0.05$. **g-h**, Same as **e-f** but along the mediolateral and ventral-dorsal axes. $*P < 0.05$. Unlabeled comparisons = not significantly different. C: caudal, D: dorsal, M: medial, R: rostral, V: ventral.

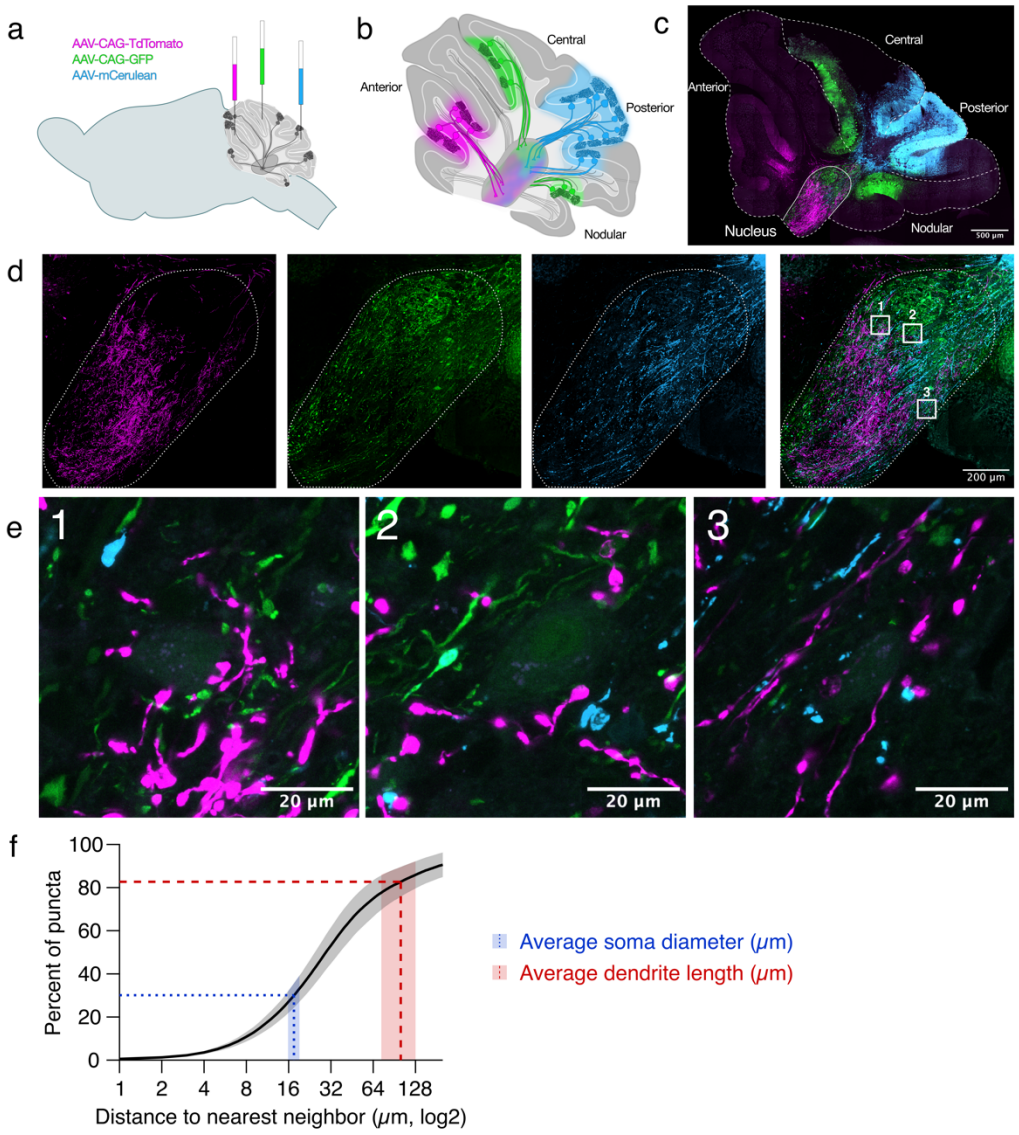


**Figure 5**: Purkinje cell puncta from different zones terminate in close proximity in the CN. **a**, Cartoon representing intracranial injections of fluorescent viruses into different areas of the cerebellar vermis. **b**, Cartoon representing Purkinje cells labeled with virus injections depicted in **c**, representative image of cerebellum with viruses expressed in different zones at 20x magnification. **d**, Expansion of nucleus in **c** showing that Purkinje cells from different lobules target different areas of the CN, 20x magnification. **e**, Expansion of numbered boxes in **d**, showing Purkinje cell puncta from different zones in apposition to individual CN neurons, 63x

magnification. **f**, Cumulative probability of nearest neighbor distance of Purkinje cell puncta from different zones. Dashed lines: average soma diameter (blue, 17.5 microns) and dendrite length (red, 100.5 microns). Shaded rectangles: 95% confidence interval of nearest neighbor puncta across animals. N = 6 animals.

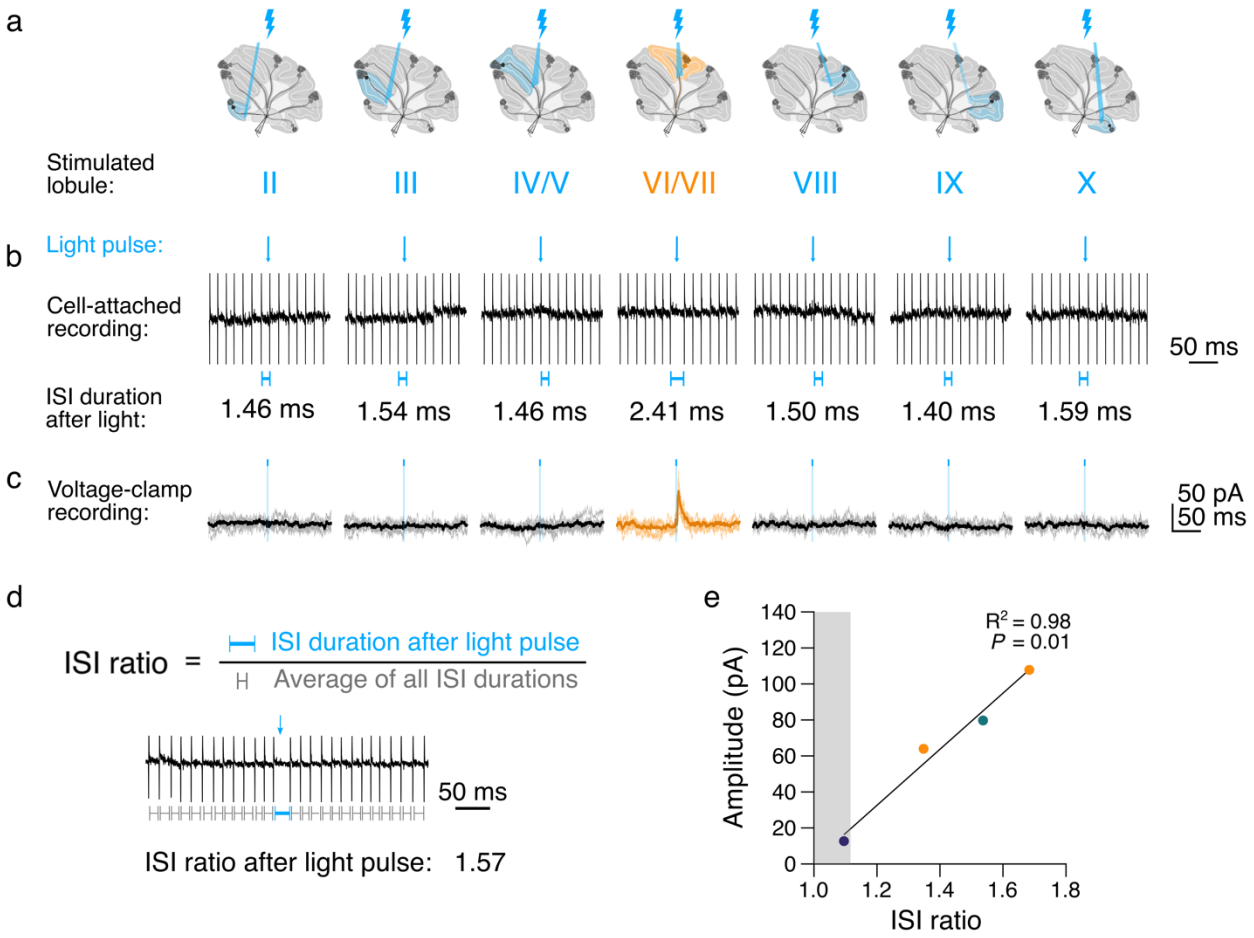


**Figure 6**: Small inputs from a single lobule are sufficient to alter CN output. **a**, Stimulation protocol. **b**, Top, representative traces of spontaneous firing from a CN neuron during lobule stimulation before breaking into whole-cell configuration. Blue line with arrowhead indicates onset and duration of light pulse. Bottom, blue lines indicate duration of inter-spike interval (ISI) immediately following stimulation. **c**, Voltage-clamp traces during stimulation from cell in **b** after breaking through to whole-cell configuration. **d**, Top, ISI ratio calculated by dividing the ISI duration after stimulation with the average ISI duration per cell per trial. Bottom, example trace from a cell with an ISI ratio of 1.57. **e**, ISI ratio vs. IPSC amplitude per cell, Pearson's $R^2$ correlation coefficient. Shaded area depicts 95% confidence interval of the ISI ratio of non-responsive lobules ($\geq 1$).